J|A|C|S
ARTICLES
Published on Web 12/07/2006

Electronic Communication and Negative Binding Cooperativity in Diborylated Bithiophenes

Anand Sundararaman,[†] Krishnan Venkatasubbaiah,[†] Maria Victor,[†] Lev N. Zakharov,[‡,§] Arnold L. Rheingold,[‡] and Frieder Jäkle*,[†]

Contribution from the Department of Chemistry, Rutgers University-Newark, 73 Warren Street, Newark, New Jersey 07102, and Department of Chemistry and Biochemistry, University of California, San Diego, La Jolla, California 92093

Received June 29, 2006; E-mail: fjaekle@rutgers.edu

Abstract: The bifunctional conjugated organoboranes Ar_2B—bt—BAr_2, which contain 2,2′-bithiophene (bt) linkers and different aryl substituents on boron (**3**: Ar = *p*-^{t}BuC$_6$H$_4$; **4**: Ar = C_6F_5; **5**: Ar = C_6F_5, Fc; Fc = ferrocenyl), have been synthesized. The electronic communication between the boron centers and cooperativity effects in the binding of pyridine have been investigated by a comprehensive study using X-ray crystallography, DFT calculations, cyclic voltammetry, ^{1}H and ^{19}F NMR, and UV visible absorption and emission spectroscopy. A comparison of the single-crystal X-ray structures of **4** and **4Py$_2$** revealed a strongly diminished bond alternation in the thiophene rings for **4**, indicative of a high degree of electronic delocalization. DFT calculations are in good agreement with the structural features determined from the X-ray analysis and, consistent with the experimental absorption and emission data, predict a smaller HOMO−LUMO gap for green luminescent **4** in comparison to blue luminescent **3**. The complexation of pyridine to the two boron centers was further investigated by ^{1}H and ^{19}F NMR for **4** and by ^{1}H NMR and UV−visible absorption spectroscopy for **3**. We found that binding of the first pyridine molecule to one of the boryl groups significantly lowers the Lewis acidity of the other boryl group. For **3**, the interaction parameter *a*, which provides a measure of communication between the boron sites, was determined to be $a = 0.23$ by UV−visible titration and 0.21 by ^{1}H NMR spectroscopy. Further enhanced electronic communication was observed for the more highly Lewis acidic fluorinated derivative **4**, for which $a = 0.025$ according to ^{19}F and ^{1}H NMR spectroscopy.

Introduction

Conjugated organic oligomers and polymers have been established as an important class of new materials with many exciting applications, for example, in electroluminescent devices, organic field effect transistors, and smart electrochromic windows.[1] Much research has also been devoted to the design and development of related hybrid systems, in which the properties of organic π-systems are combined with the unique features of semimetals or metal complexes leading to a wide range of new materials with intriguing properties.[2] In this regard, the incorporation of electron-deficient boron centers into organic structures with extended π-conjugation has attracted attention following the observation that overlap between the empty p-orbital on boron and the extended π-system frequently leads to unusual optical and electronic properties.[3,4] One of the most appealing aspects is that the presence of highly Lewis acidic centers provides an opportunity to design new sensors for Lewis basic substrates.[5,6] For instance, Yamaguchi et al. reported on a series of tri-9-anthrylborane derivatives and their effective use as fluoride sensor materials;[5c] many other borane derivatives have since been investigated. Chujo and co-workers described the use of a phenylene-vinylene-borane type p−π conjugated organoboron polymer as a fluorescent fluoride sensor and

[†] Rutgers University Newark.
[‡] University of California, San Diego.
[§] Current address: University of Oregon, Department of Chemistry, Eugene, OR, 97403-1253.

(1) (a) Skotheim, T. A., Elsenbaumer, R. L., Reynolds, J. R., Eds. *Handbook of Conducting Polymers*, 2nd ed.; Marcel Dekker, Inc.: New York, 1997. (b) Fichou, D., Ed. *Handbook of Oligo- and Polythiophenes*; Wiley-VCH: Weinheim, 1999. (c) Hadziioannou, G., van Hutten, P. F., Eds. *Semiconducting Polymers*; Wiley-VCH: Weinheim, 2000. (d) Nalwa, H. S., Ed. *Handbook of Advanced Electronic and Photonic Materials and Devices, Volume 8: Conducting Polymers*; Academic Press: San Diego, 2001. (e) Wallace, G. G.; Spinks, G. M.; Kane-Maguire, L. A. P. *Conductive Electroactive Polymers: Intelligent Materials Systems*, 2nd ed.; CRC Press: Boca Raton, FL, 2002. (f) Friend, R. H. *Pure Appl. Chem.* **2001**, *73*, 425−430. (g) Pron, A.; Rannou, P. *Progr. Polym. Sci.* **2002**, *27*, 135−190.

(2) (a) Abd-El-Aziz, A. S.; Carraher, C. E., Jr.; Pittman, C. U., Jr.; Sheats, J. E.; Zeldin, M. *Macromolecules Containing Metal and Metal-Like Elements, Volume 1, A Half-Century of Metal- and Metalloid-Containing Polymers*; John Wiley & Sons: Hoboken, NJ, 2003. (b) Manners, I. *Synthetic Metal-Containing Polymers*; Wiley-VCH: Weinheim, 2004. (c) Chandrasekhar, V. *Inorganic and Organometallic Polymers*; Springer-Verlag: New York, 2005. (d) Brook, M. A. *Silicon in Organic, Organometallic, and Polymer Chemistry*; Wiley-VCH: New York, 2000. (e) Hockemeyer, J.; Castel, A.; Riviere, P.; Satge, J.; Ryder, K. G.; Drury, A.; Davey, A. P.; Blau, W. J. *Appl. Organomet. Chem.* **1997**, *11*, 513−521. (f) Pickup, P. G. *J. Mater. Chem.* **1999**, *9*, 1641−1653. (g) Matsumi, N.; Chujo, Y. *Spec. Publ. R. Soc. Chem.* **2000**, *253*, 51−58. (h) Yamaguchi, S.; Tamao, K. *Silicon-Containing Polym.* **2000**, 461−498. (i) Wolf, M. O. *Adv. Mater.* **2001**, *13*, 545−553. (j) Puddephatt, R. J. *Coord. Chem. Rev.* **2001**, *216−217*, 313−332. (k) Nishihara, H. *Adv. Inorg. Chem.* **2002**, *53*, 41−86. (l) Yamaguchi, S.; Tamao, K. *J. Organomet. Chem.* **2002**, *653*, 223−228. (m) Hissler, M.; Dyer, P. W.; Reau, R. *Coord. Chem. Rev.* **2003**, *244*, 1−44. (n) Moorlag, C.; Sih, B. C.; Stott, T. L.; Wolf, M. O. *J. Mater. Chem.* **2005**, *15*, 2433−2436. (o) Jäkle, F. *Coord. Chem. Rev.* **2006**, *250*, 1107−1121.

10.1021/ja064396b CCC: $33.50

reported a considerable signal amplification effect.[6a] We recently developed a new family of luminescent organoboron polymers, in which Lewis acidic boron sites are embedded into the main chain of polythiophenes.[7] We observed highly efficient fluorescence quenching upon coordination of very small amounts of pyridine with an amplification factor of ca. 12 relative to a molecular model. One of the key questions with regard to the sensing behavior of such polymers is whether individual recognition sites along the polymer backbone act independently or in a cooperative fashion. The latter may provide important information on the origin of the observed sensor signal amplification.[8]

In the present study, bifunctional organoboranes with a bithiophene linker have been chosen as a model system that represents a fragment of a conjugated organoboron polymer and allows us to carefully study the cooperativity between adjacent Lewis acid sites. Previous electrochemical studies by Kaim and co-workers on phenylene-bridged diboranes of the type $Mes_2B-(C_6H_4)_n-BMes_2$ (n = 1,2; Mes = 2,4,6-trimethylphenyl) indicated a considerable degree of electronic communication between the two boron centers as reflected in two distinct reduction waves that are separated by 0.69 and 0.25 V, respectively, in the presence of a phenylene or 4,4′-biphenylene bridge.[9] A significant contribution of the quinoid resonance structure in the doubly reduced species was postulated. More recently, Shirota and co-workers have shown that the thiophene analogue 5,5′-bis(dimesitylboryl)-2,2′-bithiophene also displays two sequential cathodic waves with a considerable redox splitting.[10] However, interactions between the boron centers in these and other diboron species[5b,11] have in the past been studied almost exclusively by cyclic voltammetry. Sequential fluoride binding to arylborane oligomers has been investigated by Yamaguchi et al. for a system containing four boron centers in two different environments.[5c] Noteworthy is also some very recent work by Li and Fang and co-workers and by Baumgartner and co-workers, who reported on the use of diborylated aromatic species as luminescent fluoride sensors while these studies have been under way.[5q,r,12] Li and Fang showed that the diborylated species $Mes_2B-Th-HC{=}CH-Ph-HC{=}CH-Th-BMes_2$ acts as an efficient sensor based on two-photon excited fluorescence.[5q] They found that fluoride binds sequentially in THF with binding constants of log $K_1 = 5.51$ and log $K_2 = 5.08$, which indicate moderate cooperativity ($K_2/K_1 = 0.37$). Baumgartner and co-workers reported on a highly stable dithienophosphole oxide system with two Bpin (pin = pinacolato) substituents that can be effectively used as a ratiometric probe.[5r] The diboryldithienophosphole oxide sequentially binds fluoride with log $K_1 = 4.02$ and log $K_2 = 3.79$, corresponding to the even smaller cooperativity of $K_2/K_1 = 0.59$.

We describe here the preparation, structural, and photophysical characterization of highly Lewis acidic bifunctional conjugated organoboranes $Ar_2B-bt-BAr_2$ (**3**: Ar = *p*-^{t}BuC$_6$H$_4$; **4**: Ar = C$_6$F$_5$; **5**: Ar = C$_6$F$_5$, Fc; bt = 2,2′-bithiophene, Fc = ferrocenyl). We further discuss the electronic communication between the boron centers and the ensuing strong negative binding cooperativity, which have been studied by X-ray

(3) For reviews, see: (a) Entwistle, C. D.; Marder, T. B. *Angew. Chem., Int. Ed.* **2002**, *41*, 2927−2931. (b) Entwistle, C. D.; Marder, T. B. *Chem. Mater.* **2004**, *16*, 4574−4585. (c) Jäkle, F. Boron: Organoboranes. In *Encyclopedia of Inorganic Chemistry*, 2nd ed.; King, R. B., Ed.; Wiley: Chichester, 2005. (d) Yamaguchi, S.; Wakamiya, A. *Pure Appl. Chem.* **2006**, *78*, 1413−1424. Recent examples: (e) Lee, B. Y.; Wang, S.; Putzer, M.; Bartholomew, G. P.; Bu, X.; Bazan, G. C. *J. Am. Chem. Soc.* **2000**, *122*, 3969−3970. (f) Liu, Z.-Q.; Fang, Q.; Wang, D.; Xue, G.; Yu, W.-T.; Shao, Z.-S.; Jiang, M.-H. *Chem. Commun.* **2002**, 2900−2901. (g) Liu, Z.-Q.; Fang, Q.; Cao, D.-X.; Wang, D.; Xu, G.-B. *Org. Lett.* **2004**, *6*, 2933−2936. (h) Jia, W.-L.; Bai, D.-R.; McCormick, T.; Liu, Q.-D.; Motala, M.; Wang, R.-Y.; Seward, C.; Tao, Y.; Wang, S. *Chem.−Eur. J.* **2004**, *10*, 994−1006. (i) Kim, S.; Song, K.-H.; Kang, S. O.; Ko, J. *Chem. Commun.* **2004**, 68−69. (j) Jia, W. L.; Feng, X. D.; Bai, D. R.; Lu, Z. H.; Wang, S.; Vamvounis, G. *Chem. Mater.* **2005**, *17*, 164−170. (k) Cao, H.; Ma, J.; Zhang, G.; Jiang, Y. *Macromolecules* **2005**, *38*, 1123−1130. (l) Ulrich, G.; Goze, C.; Guardigli, M.; Roda, A.; Ziessel, R. *Angew. Chem., Int. Ed.* **2005**, *44*, 3694−3698. (m) Charlot, M.; Porrès, L.; Entwistle, C. D.; Beeby, A.; Marder, T. B.; Blanchard-Desce, M. *Phys. Chem. Chem. Phys.* **2005**, *7*, 600−606. (n) Agou, T.; Kobayashi, J.; Kawashima, T. *Org. Lett.* **2005**, *7*, 4373−4376. (o) Zhang, H.; Huo, C.; Zhang, J.; Zhang, P.; Tian, W.; Wang, Y. *Chem. Commun.* **2006**, 281−283. (p) Yuan, Z.; Entwistle, C. D.; Collings, J. C.; Albesa-Jové, D.; Batsanov, A. S.; Howard, J. A. K.; Kaiser, H. M.; Kaufmann, D. E.; Poon, S.-Y.; Wong, W.-Y.; Jardin, C.; Fathallah, S.; Boucekkine, A.; Halet, J.-F.; Taylor, N. J.; Marder, T. B. *Chem.−Eur. J.* **2006**, *12*, 2758−2771. (q) Stahl, R.; Lambert, C.; Kaiser, C.; Wortmann, R.; Jakober, R. *Chem.−Eur. J.* **2006**, *12*, 2358−2370. See also citations in ref 5.

(4) For recent examples of tricoordinate organoboron polymers, see: (a) Matsumi, N.; Naka, K.; Chujo, Y. *J. Am. Chem. Soc.* **1998**, *120*, 5112−5113. (b) Matsumi, N.; Naka, K.; Chujo, Y. *J. Am. Chem. Soc.* **1998**, *120*, 10776−10777. (c) Matsumoto, F.; Matsumi, N.; Chujo, Y. *Polym. Bull.* **2001**, *46*, 257−262. (d) Kobayashi, H.; Sato, N.; Ichikawa, Y.; Miyata, M.; Chujo, Y.; Matsuyama, T. *Synth. Met.* **2003**, *135−136*, 393−394. (e) Corriu, R. J.-P.; Deforth, T.; Douglas, W. E.; Guerrero, G.; Siebert, W. S. *Chem. Commun.* **1998**, 963−964. (f) Heilmann, J. B.; Scheibitz, M.; Qin, Y.; Sundararaman, A.; Jäkle, F.; Kretz, T.; Bolte, M.; Lerner, H.-W.; Holthausen, M. C.; Wagner, M. *Angew. Chem., Int. Ed.* **2006**, *45*, 920−925. See also citations in ref 6.

(5) (a) Yamaguchi, S.; Shirasaka, T.; Tamao, K. *Org. Lett.* **2000**, *2*, 4129−4132. (b) Yamaguchi, S.; Akiyama, S.; Tamao, K. *J. Am. Chem. Soc.* **2000**, *122*, 6335−6336. (c) Yamaguchi, S.; Akiyama, S.; Tamao, K. *J. Am. Chem. Soc.* **2001**, *123*, 11372−11375. (d) Yamaguchi, S.; Shirasaka, T.; Akiyama, S.; Tamao, K. *J. Am. Chem. Soc.* **2002**, *124*, 8816−8817. (e) Yamaguchi, S.; Akiyama, S.; Tamao, K. *J. Organomet. Chem.* **2002**, *652*, 3−9. (f) Cooper, C. R.; Spencer, N.; James, T. D. *Chem. Commun.* **1998**, 1365−1366. (g) Jia, W.-L.; Song, D.; Wang, S. *J. Org. Chem.* **2003**, *68*, 701−705. (h) Kubo, Y.; Yamamoto, M.; Ikeda, M.; Takeuchi, M.; Shinkai, S.; Yamaguchi, S.; Tamao, K. *Angew. Chem., Int. Ed.* **2003**, *42*, 2036−2040. (i) Solé, S.; Gabbaï, F. P. *Chem. Commun.* **2004**, 1284−1285. (j) Melaimi, M.; Gabbaï, F. P. *J. Am. Chem. Soc.* **2005**, *127*, 9680−9681. (k) Zhao, J.; James, T. D. *J. Mater. Chem.* **2005**, *15*, 2896−2901. (l) Zhao, J.; James, T. D. *Chem. Commun.* **2005**, 1889−1891. (m) Zhu, L.; Zhong, Z.; Anslyn, E. V. *J. Am. Chem. Soc.* **2005**, *127*, 4260−4269. (n) Koskela, S. J. M.; Fyles, T. M.; James, T. D. *Chem. Commun.* **2005**, 945−947. (o) Kubo, Y.; Ishida, T.; Kobayashi, A.; James, T. D. *J. Mater. Chem.* **2005**, *15*, 2889−2895. (p) Bresner, C.; Aldridge, S.; Fallis, I. A.; Jones, C.; Ooi, L.-L. *Angew. Chem., Int. Ed.* **2005**, *44*, 3606−3609. (q) Liu, Z.-Q.; Shi, M.; Li, F.-Y.; Fang, Q.; Chen, Z.-H.; Yi, T.; Huang, C.-H. *Org. Lett.* **2005**, *7*, 5481−5484. (r) Neumann, T.; Dienes, Y.; Baumgartner, T. *Org. Lett.* **2006**, *8*, 495−497. (s) Liu, X. Y.; Bai, D. R.; Wang, S. *Angew. Chem., Int. Ed.* **2006**, *45*, 5475−5478. (t) Hudnall, T. W.; Melaimi, M.; Gabbaï, F. P. *Org. Lett.* **2006**, *8*, 2747−2749. (u) Melaimi, M.; Solé, S.; Chiu, C.-W.; Wang, H.; Gabbaï, F. P. *Inorg. Chem.* **2006**, *45*, 8136−8143. (v) Thanthiriwatte, K. S.; Gwaltney, S. R. *J. Phys. Chem. A* **2006**, *110*, 2434−2439.

(6) Polymeric organoboron sensor systems: (a) Miyata, M.; Chujo, Y. *Polym. J.* **2002**, *34*, 967−969. (b) Sundararaman, A.; Victor, M.; Varughese, R.; Jäkle, F. *J. Am. Chem. Soc.* **2005**, *127*, 13748−13749. (c) Parab, K.; Venkatasubbaiah, K.; Jäkle, F. *J. Am. Chem. Soc.* **2006**, *128*, 12879−12885.

(7) See ref 6b.

(8) McQuade, D. T.; Pullen, A. E.; Swager, T. M. *Chem. Rev.* **2000**, *100*, 2537−2574.

(9) (a) Kaim, W.; Schulz, A. *Angew. Chem., Int. Ed. Engl.* **1984**, *23*, 615−616. (b) Schulz, A.; Kaim, W. *Chem. Ber.* **1989**, *122*, 1863−1868. (c) Lichtblau, A.; Kaim, W.; Schulz, A.; Stahl, T. *J. Chem. Soc., Perkin Trans. 2* **1992**, 1497−1501. (d) Lichtblau, A.; Hausen, H.-D.; Schwarz, W.; Kaim, W. *Inorg. Chem.* **1993**, *32*, 73−78. (e) Fiedler, J.; Zalis, S.; Klein, A.; Hornung, F. M.; Kaim, W. *Inorg. Chem.* **1996**, *35*, 3039−3043.

(10) These and related diborylated oligothiophene derivatives have been shown to act as efficient electron transport materials in organic light emitting devices (OLEDs); see: (a) Noda, T.; Shirota, Y. *J. Am. Chem. Soc.* **1998**, *120*, 9714−9715. (b) Noda, T.; Ogawa, H.; Shirota, Y. *Adv. Mater.* **1999**, *11*, 283−285. (c) Shirota, Y.; Kinoshita, M.; Noda, T.; Okumoto, K.; Ohara, T. *J. Am. Chem. Soc.* **2000**, *122*, 11021−11022. (d) Okumoto, K.; Ohara, T.; Noda, T.; Shirota, Y. *Synth. Met.* **2001**, *121*, 1655−1656. (e) Kinoshita, M.; Kita, H.; Shirota, Y. *Adv. Funct. Mater.* **2002**, *12*, 780−786. (f) Mazzeo, M.; Vitale, V.; Sala, F. D.; Anni, M.; Barbarella, G.; Favaretto, L.; Sotgiu, G.; Cingolani, R.; Gigli, G. *Adv. Mater.* **2005**, *17*, 34−39.

(11) (a) Müller, P.; Huck, S.; Köppel, H.; Pritzkow, H.; Siebert, W. *Z. Naturforsch., B: Chem. Sci.* **1995**, *50*, 1476−1484. (b) Wang, H.; Gabbai, F. P. *Organometallics* **2005**, *24*, 2898−2902. (c) Venkatasubbaiah, K.; Zakharov, L. N.; Kassel, W. S.; Rheingold, A. L.; Jäkle, F. *Angew. Chem., Int. Ed.* **2005**, *44*, 5428−5433.

(12) For cooperative effect in the binding of neutral nucleophiles to a bidentate Lewis acid, see: Chase, P. A.; Henderson, L. D.; Piers, W. E.; Parvez, M.; Clegg, W.; Elsegood, M. R. J. *Organometallics* **2006**, *25*, 349−357.

Scheme 1. Synthesis of the Diborylated Bithiophene Derivatives **3**, **4**, and **5**

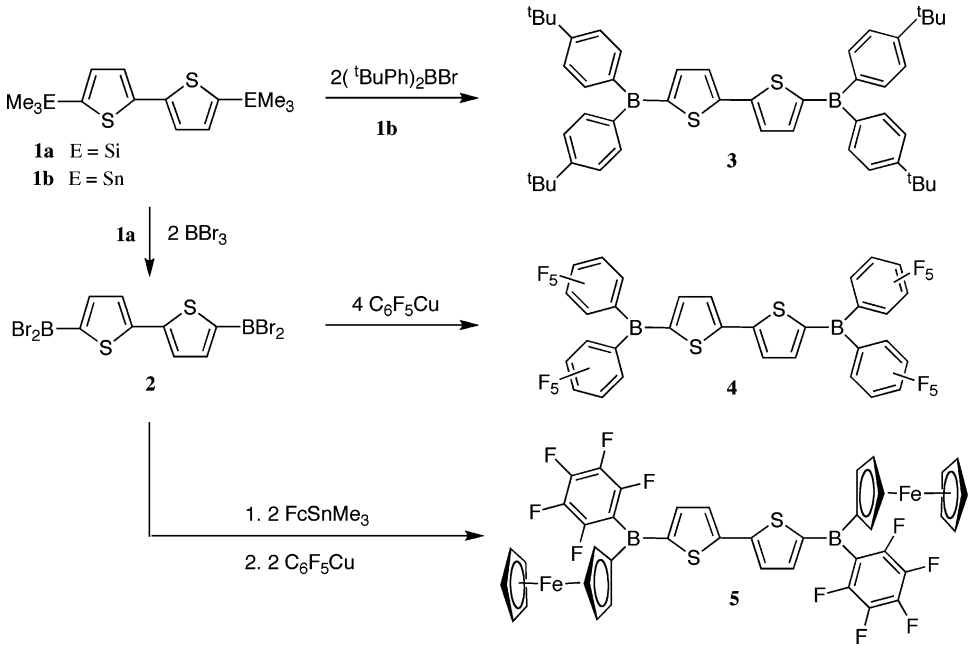

crystallography, DFT calculations, cyclic voltammetry, ^{1}H and ^{19}F NMR, and UV visible absorption and emission spectroscopy.

Results and Discussion

Synthesis of Diborylated Bithiophenes: Two different routes to the diborylated bithiophene derivatives **3**, **4**, and **5** were applied (Scheme 1). The dibromoboryl-functionalized bithiophene **2** was obtained readily via silicon−boron exchange from 2,2′-bis(trimethylsilyl)-5,5′-bithiophene (**1a**) upon reaction with BBr_3. Species **2** served as a versatile precursor to the triarylborane derivatives **4** and **5**, which were prepared through metathesis reactions with organotin and organocopper reagents (Scheme 1). Compound **4** was obtained in 71% yield by treatment of **2** with 4 equiv of pentafluorophenyl copper.[13] Reaction of **2** with $FcSnMe_3$ very selectively led to transfer of one ferrocenyl moiety to each boron center. Subsequent addition of 2 equiv of pentafluorophenyl copper gave compound **5** as a dark red solid in 77% yield. The attachment of two phenyl groups through analogous tin−boron exchange reactions is complicated by a methyl group transfer that is competing with the cleavage of the Sn−aryl bonds in $PhSnMe_3$ derivatives.[14] However, the phenyl-substituted derivative **3** was readily prepared in good yield (74%) through reaction of 2,2′-bis(trimethylstannyl)-5,5′-bithiophene (**1b**) with (tBuC_6H_4)$_2$BBr. The bifunctional triarylboranes **3**−**5** were fully characterized by multinuclear NMR spectroscopy and high-resolution mass spectrometry.

High-resolution MALDI-TOF−TOF spectra that were acquired in negative (**3**) or positive ion mode (**5**) using benzo[*a*]-pyrene as the matrix showed the molecular ion peaks with the expected isotope patterns, thus confirming the chemical composition of this class of compounds. The ^{11}B NMR spectra of compounds **3**, **4**, and **5** show resonances in the expected region for triarylboranes at 59, 56, and 51 ppm, respectively. A common feature in the ^{1}H NMR spectra is the presence of two doublets for the bithiophene linker in the region from 8.0 to 7.0 ppm. Consistent with the π-acceptor properties of tricoordinate boron, these signals are significantly downfield shifted with respect to the silylated precursor (**1a**; δ = 7.23, 7.13). The largest downfield shift is observed for **4** (δ = 7.93, 7.73), indicative of the very high Lewis acidity of the boryl groups. For compound **5** additional peaks corresponding to the expected pattern of a monoborylated ferrocene with two pseudotriplets and a singlet are observed in the range 5.0 to 4.2 ppm. The attachment of the pentafluorophenyl groups to **4** and **5** is reflected in the ^{19}F NMR spectra, both of which show a set of three resonances. It has been previously reported that the chemical shift difference $\Delta\delta_{m,p}$ between the *ortho*-F and *para*-F resonances in pentafluorophenylboranes provides an estimate of the Lewis acidity of the boron centers.[15] A comparison of $\Delta\delta_{m,p}$ for **4** and **5** further demonstrates that the attachment of two C_6F_5 groups to boron in **4** leads to a significantly higher Lewis acidity ($\Delta\delta_{m,p}$ = 11.8) relative to the mixed arylborane **5** that contains ferrocenyl and C_6F_5 groups ($\Delta\delta_{m,p}$ = 7.9).

Pyridine Binding: Complexation of the boryl groups of **3**, **4**, and **5** upon pyridine addition is evident from a strong upfield shift of the ^{11}B NMR signal to +2.7 ppm (**3**: 59 ppm), −2.6 ppm (**4**: 56 ppm), and −3.1 ppm (**5**: 51 ppm), respectively, which is indicative of tetra-coordination at boron. The boryl groups are thus readily accessible for nucleophile binding, and the respective Lewis acid−base complexes were isolated in high yields. Complex **3Py$_2$** precipitates as a white powder from toluene, complex **4Py$_2$** gives colorless crystals from CH_2Cl_2/hexanes mixtures, and the ferrocene complex **5Py$_2$** was obtained as an orange microcrystalline material upon cooling of a hot toluene solution. The isolated Lewis acid−base complexes were also completely characterized by NMR spectroscopy. Notewor-

(13) For the use of arylcopper species as aryl transfer reagents, see: Sundararaman, A.; Jäkle, F. *J. Organomet. Chem.* **2003**, *681*, 134−142.

(14) (a) Eisch, J. J.; Kotowicz, B. W. *Eur. J. Inorg. Chem.* **1998**, 761−769. (b) Cheng, X.; Slebodnick, C.; Deck, P. A.; Billodeaux, D. R.; Fronczek, F. R. *Inorg. Chem.* **2000**, *39*, 4921−4926. (c) Gamboa, J. A.; Sundararaman, A.; Kakalis, L.; Lough, A. J.; Jäkle, F. *Organometallics* **2002**, *21*, 4169−4181. (d) Boshra, R.; Sundararaman, A.; Zakharov, L. N.; Incarvito, C. D.; Rheingold, A. L.; Jäkle, F. *Chem.−Eur. J.* **2005**, *11*, 2810−2824.

(15) Piers, W. E. *Adv. Organomet. Chem.* **2005**, *52*, 1−76.

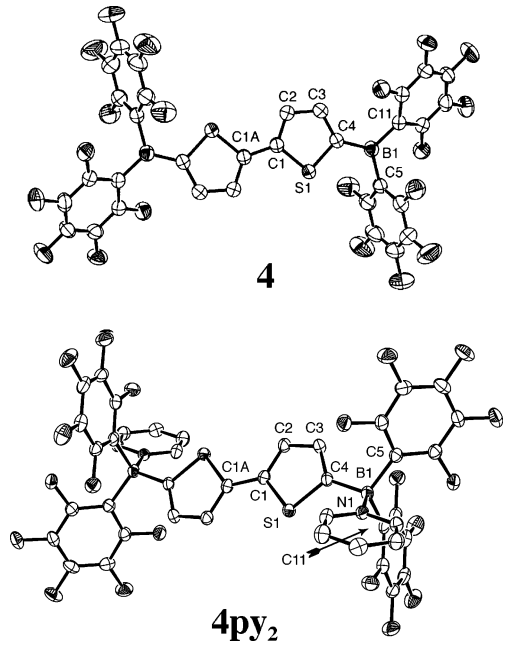

Figure 1. Molecular structures of **4** and **4Py$_2$** with thermal ellipsoids at the 50% probability level; hydrogen atoms, cocrystallized toluene (**4**), and cocrystallized mesitylene (**4py$_2$**) are omitted for clarity.

thy is that the chemical shift differences $\Delta\delta_{m,p}$ in the ^{19}F NMR spectra of **4Py$_2$** ($\Delta\delta_{m,p} = 6.4$ ppm) and **5Py$_2$** ($\Delta\delta_{m,p} = 5.5$ ppm) are considerably smaller than those for the free acids.

Treatment of the complexes **4Py$_2$** and **5Py$_2$** with the stronger Lewis acid $B(C_6F_5)_3$ in CH_2Cl_2 solution led to decomplexation and reformation of **4** and **5**, respectively, according to ^{19}F NMR spectroscopy. The reversibility of the pyridine binding also manifests itself in the FAB mass spectral data. FAB-MS analysis of **4Py$_2$** using 2-nitrophenyl octyl ether (NPOE) as the matrix revealed the presence of molecular ion peaks corresponding to the bis-adduct **4Py$_2$** (20%), the monoadduct **4Py** (25%), and the free acid **4** (42%). Interestingly, molecular ion peaks corresponding to the dimers **4$_2$Py$_4$** (0.15%) and **4$_2$Py$_3$** (0.11%) were also observed, albeit in very small amounts. For **3Py$_2$** and **5Py$_2$** only peaks corresponding to loss of pyridine could be detected, which may indicate weaker binding of pyridine in these complexes.

Structural Studies: The effect of pyridine binding on the structural parameters of diborylated bithiophene has been studied for compound **4**. Yellow needlelike single crystals of **4** were grown by recrystallization from toluene at −38 °C, and colorless rodlike crystals of the pyridine adduct **4Py$_2$** were obtained by recrystallization from hot mesitylene. The crystals of **4** contain three disordered cocrystallized toluenes, and those of **4Py$_2$**, two mesitylenes for each bithiophene molecule. The structures of **4** and **4Py$_2$** are displayed in Figure 1, and selected geometric parameters are summarized in Table 1. For both **4** and **4Py$_2$**, the molecule lies on a center of symmetry between the thiophene rings of the 2,2′-bithiophene moiety, which consequently adopt a coplanar configuration (Figure 1). The two C_6F_5 substituents are arranged in a propeller-like fashion in the free acid (**4**), a feature that is commonly observed especially for triarylboranes with bulkier groups.[16] The boron−carbon bond lengths to the

Table 1. Selected Bond Lengths [Å], Interatomic Distances [Å], and Angles [deg] for **4** and **4Py$_2$**

4		**4Py$_2$**	
B(1)−C(4)	1.507(3)	C(4)−B(1)	1.617(3)
B(1)−C(11)	1.576(3)	B(1)−C(11)	1.648(3)
B(1)−C(5)	1.578(3)	B(1)−C(5)	1.645(3)
		B(1)−N(1)	1.624(3)
S(1)−C(1)	1.703(2)	S(1)−C(1)	1.730(2)
S(1)−C(4)	1.732(2)	S(1)−C(4)	1.740(2)
C(1)−C(2)	1.372(3)	C(1)−C(2)	1.363(3)
C(2)−C(3)	1.390(3)	C(2)−C(3)	1.417(3)
C(3)−C(4)	1.383(3)	C(3)−C(4)	1.359(3)
C(1)−C(1A)	1.445(4)	C(1)-C(1A)	1.448(3)
C(4)−B(1)−C(11)	122.5(2)	C(4)−B(1)−C(11)	105.4(1)
C(4)−B(1)−C(5)	118.6(2)	C(4)−B(1)−C(5)	110.0(2)
C(11)−B(1)−C(5)	118.9(2)	C(11)−B(1)−C(5)	116.5(2)
C(2)−C(1)−C(1A)	128.3(3)	C(2)−C(1)−C(1A)	129.5(2)
C(11)−B(1)−C(4)−S(1)	−171.5(2)	C(11)−B(1)−C(4)−S(1)	61.5(2)
C(5)−B(1)−C(4)−S(1)	9.4(3)	C(5)−B(1)−C(4)−S(1)	−172.1(1)
C(1−4)S(1) // C(5−10)	69.4(1)	C(1−4)S(1) // C(5−10)	61.07(6)
C(1−4)S(1) // C(11−16)	44.0(1)	C(1−4)S(1) // C(11−16)	84.58(5)
C(5−10) // C(11−16)	89.0(1)	C(5−10) // C(11−16)	56.35(6)
		C(1−4)S(1) // N1C(17−21)	52.96(6)

C_6F_5 groups are B1−C11 = 1.576(3) Å and B1−C5 = 1.578(3) Å, respectively. In comparison, the B1−C4 distance to the more electron-rich bithiophene moiety of 1.507(3) Å is significantly shorter, indicating a stronger π-bonding of the trivalent boron centers to the bithiophene rings than to the C_6F_5 groups. Upon binding of pyridine, all of the B−C bonds become significantly longer as the hybridization on boron changes to sp^3. While the B−C bonds to the bithiophene moiety (1.617(3) Å) in **4Py$_2$** remain shorter than those to the C_6F_5 groups (1.648(3) and 1.645(3) Å), the difference is smaller than that for the free acid **4**. A strong effect of the Lewis acidic boron centers on the carbon−carbon distances within the thiophene rings is noteworthy. In contrast to most other bithiophene derivatives, for the free acid **4** the C−C distances within the thiophene rings are quite similar to one another (all within 1.372(3) to 1.390(3) Å). However, a distinct bond alternation is observed for the pyridine complex **4Py$_2$** with two short distances (C(1)−C(2) = 1.363(3) Å and C(3)−C(4) = 1.359(3) Å) and one longer distance (C(2)−C(3) = 1.417(3) Å), which is typical of bithiophenes. The carbon−carbon distance between the two central thiophene rings of 1.445(4) Å in **4** is similar to that of 1.448(3) Å in **4Py$_2$**.[17]

It is also interesting to note that the packing diagram of **4** reveals π-stacking interactions between one of the cocrystallized toluene solvent molecules and the bithiophene moiety, leading to extended stacks in the direction of the crystallographic *a*-axis (Figure 2). The distance between the average planes of the aromatic rings is ca. 3.47 Å, indicative of strong arene−arene interactions.[18,19] Another cocrystallized toluene solvent molecule also forms π-stacking interactions, but with the aromatic rings

(16) (a) Blount, J. F.; Finocchiaro, P.; Gust, D.; Mislow, K. *J. Am. Chem. Soc.* **1973**, *95*, 7019−7029. (b) Toyota, S.; Asakura, M.; Oki, M.; Toda, F. *Bull. Chem. Soc. Jpn.* **2000**, *73*, 2357−2362. (c) See ref 3p.

(17) A Cambridge Structure Database search gave a mean C−C distance of 1.449 Å for other bithiophene derivatives.

(18) Alternating stacks of electron-deficient fluorinated arenes with arenes are more common; for example, see: (a) Williams, J. H. *Acc. Chem. Res.* **1993**, *26*, 593−598. (b) Pratt Brock, C.; Naae, D. G.; Goodhand, N.; Hamor, T. A. *Acta Crystallogr.* **1978**, *B34*, 3691−3696. (c) Coates, G. W.; Dunn, A. R.; Henling, L. M.; Dougherty, D. A.; Grubbs, R. H. *Angew. Chem., Int. Ed. Engl.* **1997**, *36*, 248−251. (d) Bartholomew, G. P.; Bu, X.; Bazan, G. C. *Chem. Mater.* **2000**, *12*, 2311−2318. (e) Collings, J. C.; Batsanov, A. S.; Howard, J. A. K.; Marder, T. B. *Acta Crystallogr.* **2001**, *C57*, 870−872. (f) Collings, J. C.; Roscoe, K. P.; Thomas, R. L.; Batsanov, A. S.; Stimson, L. M.; Howard, J. A. K.; Marder, T. B. *New J. Chem.* **2001**, *25*, 1410−1417. (g) Collings, J. C.; Roscoe, K. P.; Robins, E. G.; Batsanov, A. S.; Stimson, L. M.; Howard, J. A. K.; Clark, S. J.; Marder, T. B. *New J. Chem.* **2002**, *26*, 1740−1746.

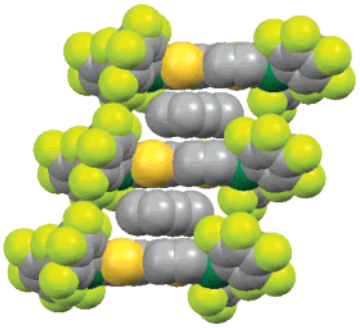

Figure 2. Space filling diagram of **4** showing the formation of stacks along the crystallographic *a*-axis through π-interactions between the bithiophene moiety and one of the toluene molecules. The other toluene molecules are omitted for clarity.

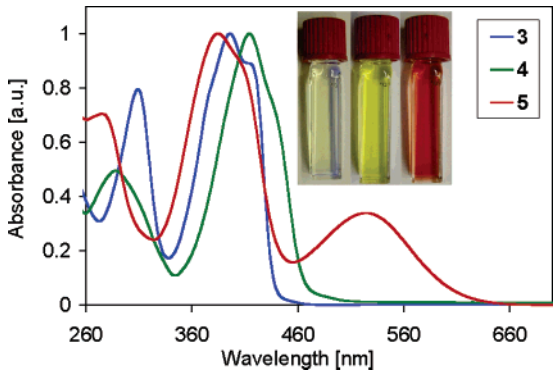

Figure 3. Absorption spectra of **3**, **4**, and **5** in CH_2Cl_2 solution.

of C_6F_5 groups (see Supporting Information). Both toluene solvent molecules are disordered over two positions, and only the one that forms stacks with the bithiophene moiety is shown in Figure 2.

Photophysical Properties and Quantum Chemical Calculations: Compounds **3**, **4**, and **5** display interesting photophysical properties in solution and the solid state. While **3** is almost colorless, compound **4** is yellow and the ferrocene derivative **5** is dark red colored (Figure 3). The spectra of the diborylated bithiophenes in dichloromethane display strong absorption bands in the UV, which reach into the visible region of the spectrum. These bands are observed for **3** at $\lambda_{max} = 396$ nm ($\epsilon = 48\,290$), for **4** at $\lambda_{max} = 413$ nm ($\epsilon = 31\,400$), and for **5** at $\lambda_{max} = 387$ nm ($\epsilon = 23\,890$) (Table 2). Interestingly, the absorption maxima seem to experience a bathochromic shift with enhanced Lewis acidity, which based on the electronic nature of the substituents is anticipated to increase in the order **5** < **3** < **4**. A red-shifted shoulder is another common feature in the spectra for these compounds. In addition, compound **5** shows a relatively strong band at 524 nm, which is typical of d−d transitions with considerable charge-transfer character in ferrocenylboranes.[14c,20]

For **3** and **4**, a trend similar to that for the absorption maxima is also observed for the emission spectra (Figure 4). A strong blue emission with maxima at $\lambda_{em,max} = 436$ and 461 nm is evident upon excitation of a CH_2Cl_2 solution of **3** (quantum efficiency $\Phi = 0.79$). These data are comparable to those reported by Shirota for the mesityl derivative $Mes_2B-bt-BMes_2$

Table 2. UV−visible Absorption and Emission Data

diborylated bithiophene	**3**	**4**	**5**
$\lambda_{abs,max}$ [nm], CH_2Cl_2	306, 396, 411[a]	287, 413, 437[a]	276, 387, 406[a], 524[b]
log ϵ [M^{-1} L^{-1}], CH_2Cl_2	4.57, 4.68, 4.63	4.09, 4.50, 4.34	4.26, 4.38, 4.36, 3.97
$\lambda_{em,max}$ [nm], CH_2Cl_2[d]	436, 461	476, 495[a]	*c*
$\lambda_{em,max}$ [nm], solid[d]	472, 485[a]	525, 547[a]	*c*
Φ[e], CH_2Cl_2	0.79	0.03	*c*

[a] Shoulder. [b] d−d transition. [c] Emission quenched due to iron center of ferrocene. [d] Excited at λ_{max}. [e] Measured relative to anthracene. Concentrations were 5.57×10^{-7} M for **3**, 5.85×10^{-5} M for **4**, and 9.44×10^{-5} M for **5**.

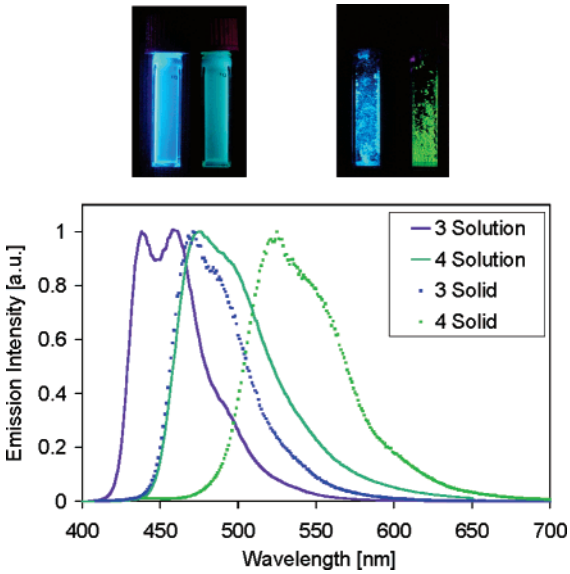

Figure 4. Emission spectra of **3** and **4** in CH_2Cl_2 solution and in the solid state.

with fluorescence maxima at $\lambda_{max} = 446$, 442 nm.[10a,b] In contrast, the emission maximum of compound **4** is shifted by ca. 40 nm to $\lambda_{em,max} = 476$ nm and the quantum efficiency is much lower with $\Phi = 0.03$.

In comparison to the solution maxima, the emissions of **3** and **4** experience a bathochromic shift in the solid state of ca. 35 and 50 nm, respectively (Table 2, Figure 4). Similarly, the solid-state excitation edge of **3** and **4** is red-shifted by 60 to 70 nm in comparison to the solution absorption edge. This phenomenon is consistent with the observation that the central bithiophene unit adopts a coplanar structure in the solid state, while in solution other ring-twisted conformations also contribute. However, intermolecular $\pi-\pi$ interactions, as deduced from the single-crystal X-ray structure of **4**, likely also impact the photophysical properties in the solid state.[21]

The considerable bathochromic shift for the perfluorinated analogue, both in the absorption and fluorescence spectra, can be attributed to the strongly electron-withdrawing nature of the C_6F_5 substituents, which leads to a higher Lewis acidity of the boron centers and thus to stronger p−π interactions with the bithiophene moiety in **4**. The latter is expected to lead to stabilization of the quinoid resonance structure and hence a lowering of the HOMO−LUMO gap. DFT calculation have

(19) For an example of the use of mesitylene to fill structural voids and thus aid in the crystallization of compound $Mes_2B-(anthracenediyl)-BMes_2$, see: Yuan, Z.; Taylor, N. J.; Ramachandran, R.; Marder, T. B. *Appl. Organomet. Chem.* **1996**, *10*, 305−316.

(20) Carpenter, B. E.; Piers, W. E.; Parvez, M.; Yap, G. P. A.; Rettig, S. J. *Can. J. Chem.* **2001**, *79*, 857−867.

(21) For a detailed account on stacking effects in a related diborylated dithienothiophene derivative, see ref 10f.

Table 3. Comparison of Geometric Parameters from X-ray Analysis and DFT Calculations of **3**, **3Py**, **3Py$_2$**, **4**, **4Py**, and **4Py$_2$**

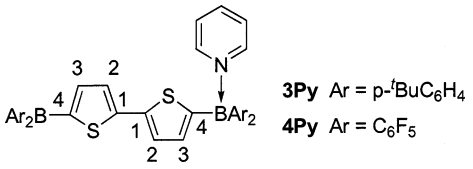

		3Py (DFT)		
	3 (DFT)	uncomplexed	complexed	**3Py$_2$** (DFT)
B−C(Ph) (Å)	1.5684	1.5706	1.6347	1.6355
	1.5674	1.5690	1.6308	1.6309
B-C4(Th) (Å)	1.5501	1.5447	1.6254	1.6219
C1−C1* (Å)	1.4472	1.4468		1.4490
C1−C2 (Å)	1.3865	1.3872	1.3799	1.3787
C2−C3 (Å)	1.4101	1.4098	1.4201	1.4218
C3−C4 (Å)	1.3898	1.3901	1.3800	1.3783
C1−S (Å)	1.7447	1.7456	1.7544	1.7558
C4−S (Å)	1.7596	1.7636	1.7612	1.7658
B−N(Py) (Å)			1.6875	1.6912

	4 (X-ray/DFT)		**4Py** (DFT)		**4Py$_2$** (X-ray/DFT)	
	X-ray	DFT	uncomplexed	complexed	X-ray	DFT
B−C(C$_6$F$_5$) (Å)	1.576(3)	1.5775	1.5825	1.6544	1.648(3)	1.6464
	1.578(3)	1.5795	1.5811	1.6480	1.645(3)	1.6517
B−C4(Th) (Å)	1.507(3)	1.5244	1.5150	1.6261	1.617(3)	1.6146
C1−C1* (Å)	1.445(4)	1.4458	1.4442		1.448(3)	1.4475
C1−C2 (Å)	1.372(3)	1.3914	1.3932	1.3806	1.363(3)	1.3775
C2−C3 (Å)	1.390(3)	1.4034	1.4019	1.3173	1.417(3)	1.4213
C3−C4 (Å)	1.383(3)	1.3934	1.3948	1.3806	1.359(3)	1.3759
C1−S (Å)	1.703(2)	1.7387	1.7394	1.7516	1.730(2)	1.7564
C4−S (Å)	1.732(2)	1.7552	1.7610	1.7584	1.740(2)	1.7652
B−N(Py) (Å)				1.6667	1.624(3)	1.6615

Table 4. Calculated Electronic Transitions for **3**, **3Py**, **3Py$_2$**, **4**, **4Py**, and **4Py$_2$** from TD-DFT (B3LYP) Calculations[a]

compound	transition	MO contributions	energy gap eV (nm)	oscillator strength *f*
3	$S_0 \rightarrow S_1$	HOMO → LUMO	2.97 (417)	1.3343
3Py	$S_0 \rightarrow S_2$	HOMO → LUMO + 1	3.05 (407)	0.9751
3Py$_2$	$S_0 \rightarrow S_{15}$	HOMO → LUMO + 4	3.65 (339)	0.9548
4	$S_0 \rightarrow S_1$	HOMO → LUMO	2.88 (430)	1.2544
4Py	$S_0 \rightarrow S_2$	HOMO → LUMO	3.01 (411)	1.0192
4Py$_2$	$S_0 \rightarrow S_7$	HOMO − 3 → LUMO	3.50 (354)	0.7582
		HOMO − 2 → LUMO + 1		
		HOMO → LUMO + 4		

[a] Only the most intense low-energy transitions are shown; for a complete list see the Supporting Information.

been performed using Gaussian03 to gain further insight into a possible correlation between the Lewis acidity of the boron centers in **3** and **4** and their optical properties (Tables 3 and 4).[22]

The calculations reproduce the structural parameters for **4** determined by single-crystal X-ray diffraction very well. A comparison of the structural features derived for **4** with those calculated for the non-fluorinated analogue **3** is of particular interest (Table 3). The most striking difference is that the B−C4 bonds to the bithiophene moiety are significantly shorter for the fluorinated derivative **4** (1.5244 Å) in comparison to **3** (1.5501 Å). Another important observation is that the bond alternation in the thiophene rings is less pronounced for **4** than in the case of **3**, indicative of enhanced electronic delocalization. Figure 5 shows the computed frontier orbitals for **3** and **4**. Pronounced overlap of the bithiophene π-system with the empty p-orbital on boron is evident for the LUMOs, while the contribution to the HOMO levels is small, though somewhat more apparent in **4** than in **3**. Both the HOMO and LUMO orbitals for the fluorinated derivative **4** are stabilized relative to those of **3** (see Table S1 in the Supporting Information). The effect is slightly stronger for the LUMO, which effectively leads to a smaller HOMO−LUMO gap for **4** (3.186 eV) relative to **3** (3.348 eV).

We next performed calculations for the monoadducts and bis-adducts of **3** and **4** with pyridine (Table 3). The results for **4Py$_2$** compare favorably with the crystal structure data. The most significant deviation from the X-ray data is that the B−N distance to the pyridine rings is slightly overestimated (DFT: 1.6615 Å; X-ray: 1.624(3) Å). Similar limitations have been reported previously for DFT calculations of other related Lewis acid−base complexes.[23] Nonetheless, all other parameters are very well reproduced by the calculations. Both the X-ray data and calculations show a lengthening of the B−C bond distances as a result of the tetracoordination of boron and a more pronounced bond alternation of the thiophene rings. Thus, the C2−C3 distances are ca. 0.04 to 0.05 Å longer than the C1−C2 and C3−C4 bonds (for the free acids: 0.02 Å for **3** and 0.01 Å for **4**). Only small differences are observed for the monocomplexed species **3Py** and **4Py** relative to the free acids and bis-adducts, respectively. However a consistent trend is found especially for **4Py**, for which the B−C(Th) bond of the uncomplexed borane is shortened relative to that of the free acid **4** and the bond alternation within the adjacent thiophene ring is nearly completely absent. This indicates that coordination of pyridine to one of the boron centers leads to enhanced overlap of the bithiophene π-system with the remaining tricoordinate boron moiety. Since this effect is much more evident for **4Py** than **3Py** stronger communication between the two binding sites should be expected for the more electron-deficient **4** (see vide infra).

Upon complexation of the boryl groups with pyridine, the nature of the HOMO and LUMO orbitals changes dramatically. Thus, for **3Py$_2$** and **4Py$_2$** the HOMO levels are significantly higher in energy and primarily centered on the bithiophene moiety without any contribution from the boron atoms (see Supporting Information). While the LUMO levels show contributions from the pyridine ligands, the LUMO + 4 orbitals are bithiophene-centered, which are 3.969 eV (**3Py$_2$**) and 3.861 eV (**4Py$_2$**) above the HOMO, respectively; the energy differences between these orbitals are thus much larger than the HOMO−LUMO gaps in the free acids (**3**, 3.348 eV; **4**, 3.186 eV). In the case of the monoadducts, **3Py** and **4Py**, the HOMO and LUMO (**4Py**)/LUMO + 1 (**3Py)** orbitals show overlap between the bithiophene moiety and the tricoordinate but not the tetracoordinate boryl groups. The HOMO and LUMO orbitals are higher in energy than those in the free acids, but the HOMO−LUMO gaps are nearly unchanged.

(22) DFT calculations were performed with the Gaussian03 program (Frisch, M. J., et al. *Gaussian03*, revision C.02; Gaussian Inc.: Wallingford CT, 2004). Geometries and electronic properties were calculated by means of the hybrid density functional B3LYP with the basis set of 6-31.G(d). The input files were generated using Gaussview except for **4Py$_2$** (input file from X-ray data). The orbital representations were generated using Gaussview.

(23) Scheibitz, M.; Bolte, M.; Bats, J. W.; Lerner, H.-W.; Nowik, I.; Herber, R. H.; Krapp, A.; Lein, M.; Holthausen, M. C.; Wagner, M. *Chem. Eur. J.* **2005**, *11*, 584−603.

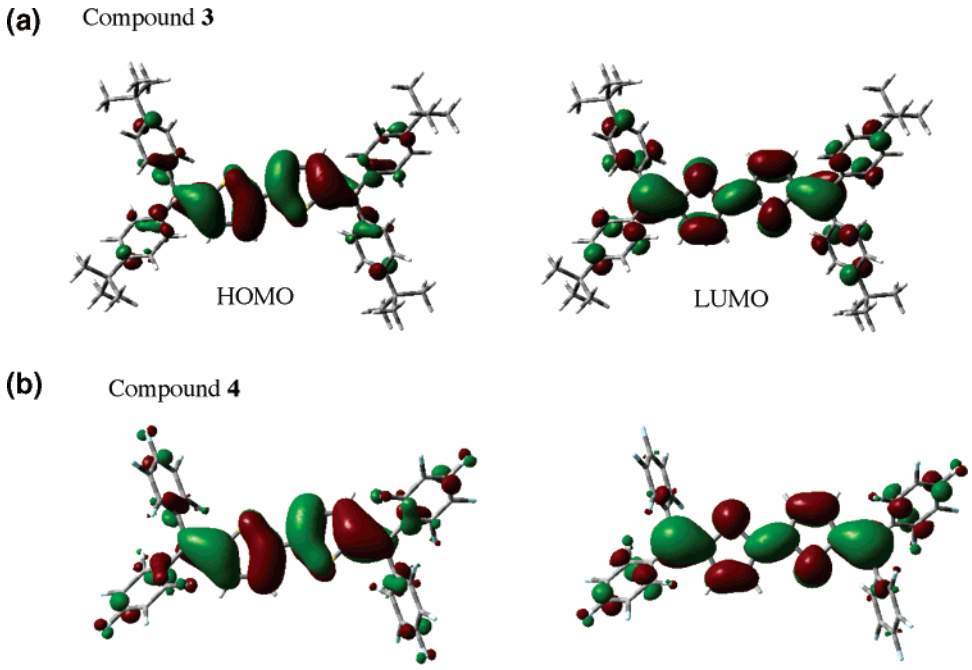

Figure 5. HOMO and LUMO diagrams of **3** and **4**. Scaling radii of 0.75 and an isovalue of 0.02 were used.

We carried out TD-DFT calculations to gain further insight into the origin of the electronic transitions for **3**, **4**, and their respective pyridine complexes (Table 4). The calculations revealed that, for both **3** and **4**, the lowest energy transition corresponds to promotion of electrons from the HOMO to the LUMO levels. The calculated excitations of 417 nm for **3** and 430 nm for **4** correlate well with the experimentally observed values for the absorption maxima λ_{max} (**3**: 411 nm; **4**: 437 nm). Importantly, the calculations nicely reproduce the red shift for the fluorinated derivative **4**.

For the bis-adducts the lowest energy transitions with high oscillator strength are the $S_0 \rightarrow S_{15}$ excitation corresponding to a HOMO→LUMO + 4 transition for $\mathbf{3Py_2}$ and the $S_0 \rightarrow S_7$ excitation for $\mathbf{4Py_2}$ with multiple orbital contributions, the primary of which is the HOMO→LUMO + 4 component. The energy for these transitions of 3.65 eV (339 nm) for $\mathbf{3Py_2}$ and of 3.50 eV (354 nm) for $\mathbf{4Py_2}$, respectively, is far higher than that for the free acid (2.97 eV for **3**; 2.88 eV for **4**). Strongly blue-shifted absorption bands are therefore expected for the bis-adducts. In contrast, the monoadducts display transitions that are only slightly higher in energy and lower in intensity than those of the free acids.

Electrochemical Studies: Cyclic voltammetry was used to investigate the electronic communication between the two ferrocene moieties in **5**. In CH_2Cl_2 with $Bu_4N[(B(C_6F_5)_4)]$ as the supporting electrolyte, compound **5** shows a reversible one-electron oxidation at −11 mV and a quasi-reversible second oxidation wave at +207 mV relative to the ferrocene/ferrocenium couple (Figure 6a). The peak separation of 218 mV can be attributed to a moderate degree of metal−metal interaction through the diborylated bithiophene linker.[24] The cyclic voltammogram of $\mathbf{5Py_2}$ on the other hand showed significantly lower redox potentials of −123 mV and −15 mV with a considerably smaller separation of $\Delta E = 108$ mV (Figure 6b). This indicates that complexation of the boron centers leads to a breakdown of conjugation[25] and, thus, a decrease in the communication through the diborylated bithiophene linker.

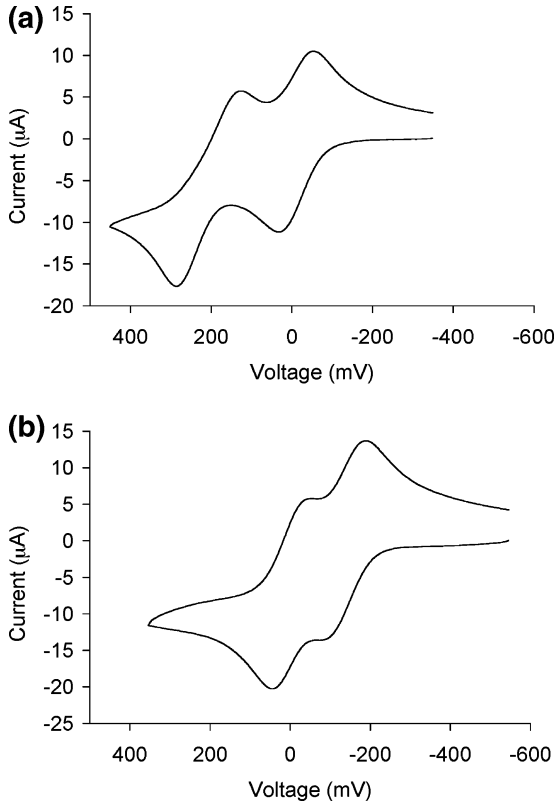

Figure 6. Cyclic voltammograms of (a) **5** and (b) $\mathbf{5Py_2}$ with 0.1 M $Bu_4N[B(C_6F_5)]_4$ in CH_2Cl_2 as the supporting electrolyte (scan rate 100 mV/s). The scans are referenced relative to the Fc/Fc^+ couple.

Pyridine Titration Studies: We performed titration studies with pyridine to further investigate the communication between

(24) Related diferrocene species that feature α,ω-dialkynylbithiophene linkers show only a single redox wave with $[Bu_4N]ClO_4$ in CH_2Cl_2 as the supporting electrolyte: Thomas, K. R. J.; Lin, J. T.; Wen, Y. S. *Organometallics* **2000**, *19*, 1008−1012.

(25) See also: Scheibitz, M.; Heilmann, J. B.; Winter, R. F.; Bolte, M.; Bats, J. W.; Wagner, M. *Dalton Trans.* **2005**, 159−170.

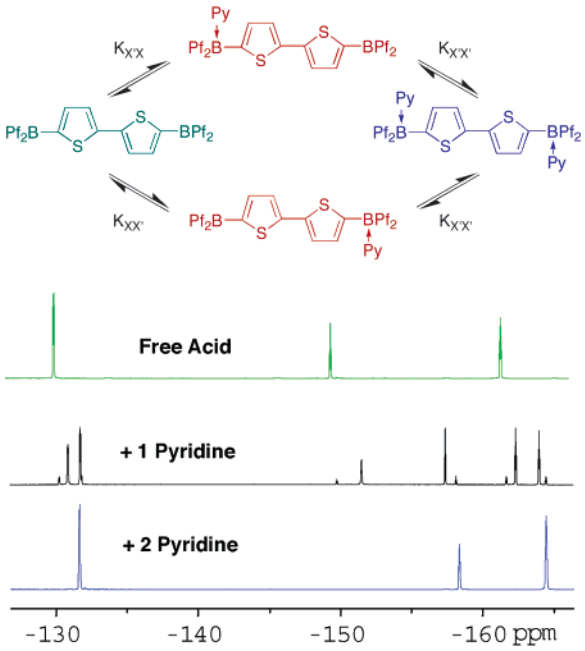

Figure 7. ^{19}F NMR plot for the titration of **4** with pyridine (Pf = C_6F_5).

the boron centers. The binding of pyridine was monitored through (a) NMR spectroscopy and (b) UV−visible and fluorescence spectroscopy.

(a) NMR Spectroscopy. Titration of compound **4** with pyridine was followed by ^{1}H and ^{19}F NMR spectroscopy. Figure 7 shows the room temperature ^{19}F NMR spectra for the free acid **4**, the mixture obtained upon addition of 1 equiv of pyridine, and the fully complexed species **4Py$_2$** that is formed in the presence of 2 equiv of pyridine. Addition of 1 equiv of pyridine resulted in the appearance of two new sets of C_6F_5 signals, which are upfield shifted in comparison to the signals of the free acid **4**. The most upfield shifted new peaks can be assigned to the C_6F_5 groups on the boron atom that is coordinated by pyridine, while the signals closer to those of the starting material **4** are assigned to the C_6F_5 groups attached to the tricoordinate boron moiety. The amount of monocomplexed diborane **4Py** was estimated by NMR integration to ca. 86% with the remainder consisting of ca. 7% of starting material and 7% of the fully complexed species **4Py$_2$**. The appearance of small amounts of **4** and **4Py$_2$** upon addition of 1 equiv of pyridine is a result of dissociation of the intermediate **4Py** into the free acid **4** and fully complexed **4Py$_2$**. In the absence of any interaction between the two boron centers one would expect a 25:50:25 statistical ratio for [**4**]:[**4Py**]:[**4Py$_2$**], which corresponds to an interaction parameter of $a = 1$, and therefore $K_{11} = 4K_{12}$ holds for the relation between the stepwise binding constants (see eqs 1 and 2).[26] For the two Lewis acid sites in **4**, the interaction parameter a, which is related to the equilibrium constant for the disproportionation process (2 **4Py** $\rightleftarrows$ **4** + **4Py$_2$**), was estimated by ^{19}F NMR to be $a = 0.025$, indicative of strong negative cooperativity. In line with this result is also the observed upfield shift of the C_6F_5 signals of the uncomplexed boron center of **4Py** relative to those of **4**. Similar analysis of the corresponding ^{1}H NMR spectra corroborated the value determined for a. In contrast, ^{1}H NMR studies for **3**, which

(26) Connors, K. A. *Binding Constants*; Wiley-Interscience: London, 1987.

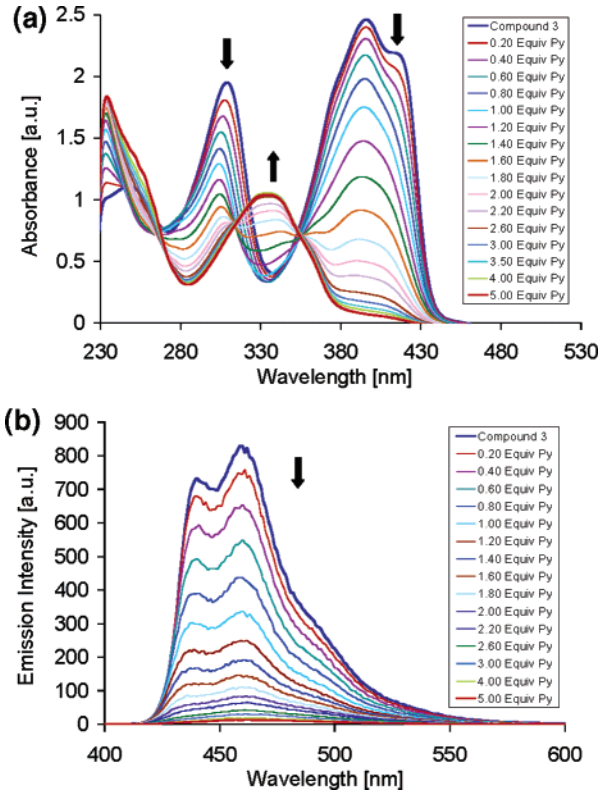

Figure 8. (a) UV−vis absorption and (b) emission plots for the titration of **3** (CH_2Cl_2, 51.9 μM) with pyridine (CH_2Cl_2, 1.49 mM).

were performed at −30 °C where the slow exchange regime is reached, gave a significantly lower value of $a = 0.21$, consistent with a less pronounced binding cooperativity.

$$K_{11} = \frac{[\text{LA Py}]}{[\text{LA}][\text{py}]} \qquad K_{12} = \frac{[\text{LA Py}_2]}{[\text{LA Py}][\text{py}]} \tag{1}$$

$$a = 4\frac{K_{12}}{K_{11}} = 4\frac{[\text{LA Py}_2][\text{LA}]}{[\text{LA Py}][\text{LA Py}]} \tag{2}$$

(b) UV−visible Absorption and Fluorescence Spectroscopy. To independently confirm the negative binding cooperativity, the pyridine binding process for **3** was further examined by titration studies, which were monitored by UV−vis absorption and fluorescence spectroscopy as illustrated in Figure 8. Sequential addition of pyridine to **3** resulted in a gradual decrease of the absorption bands at 396 nm (ϵ = 48 290) and 306 nm (ϵ = 37 160). A new high-energy absorption band developed at 333 nm (ϵ = 19 800) (Figure 8a). This process is reflected in a color change of the solution from pale yellow to colorless, which is consistent with the computational results and can be related to the interruption of the extended p−π conjugation through the two boron centers upon pyridine coordination. The emission spectra, which were acquired simultaneously, show a concomitant decrease in emission intensity indicative of static fluorescence quenching (Figure 8b).

Closer examination of the UV−visible titration data revealed that there are different regimes with separate isosbestic points, indicating that two distinct cooperative binding processes are encountered. Refinement according to a two-site binding model that considers the Lewis acid groups as two tight binding sites

was performed using the program Hyperquad. A stable refinement was obtained with binding constants log $K_{11} = 6.64 \pm 0.04$ and log $K_{12} = 5.40 \pm 0.04$. The corresponding microscopic binding constants $K_{XX'} = 0.5K_{11} = 2.2 \times 10^6\ M^{-1}$ and $K_{X'X'} = 2K_{12} = 5.0 \times 10^5\ M^{-1}$ for the first and second binding process, respectively, are in the range expected for triarylborane pyridine complexes.[27] Moreover, the cooperativity parameter $a = 0.23$ is in very good agreement with that determined by ^{1}H NMR spectroscopy ($a = 0.21$).

Summary and Conclusion

In conclusion, we have used a comprehensive set of tools that encompass X-ray crystallography, DFT calculations, cyclic voltammetry, ^{1}H and ^{19}F NMR, and UV visible absorption and emission spectroscopy to study the electronic communication and binding cooperativity of two boron centers that are separated by a conjugated bithiophene bridge. These studies show that electronic delocalization is most pronounced for the most highly Lewis acidic fluorinated derivative **4**. For instance, with enhanced Lewis acidity of boron, the B−C(Th) bonds become shorter and the bond alternation in the thiophene rings is less pronounced. Moreover, the HOMO and LUMO levels are considerably lowered, with a stronger effect on the LUMO level that leads to a narrowing of the HOMO−LUMO gap, which is also reflected in a bathochromic shift of the absorption and emission bands. Concurrent with the enhanced electronic delocalization in **4** goes a strong increase in the negative binding cooperativity between the two Lewis acid groups. Binding of pyridine to one of the boron centers significantly lowers the affinity of the other boron center for pyridine. This effect can be attributed to effective communication through the bithiophene linker and is much more pronounced for the more highly Lewis acidic **4** in comparison to **3**.

The results described in here thus provide new insight into the electronic communication in bifunctional boranes, which have important implications on the use of these systems in sensing applications and in the assembly of supramolecular structures through donor−acceptor bonding. Moreover, the consequences of electronic communication between Lewis acidic boron sites are of key importance for a complete understanding of recently developed conjugated organoboron polymers,[7] their behavior as so-called "molecular wires", and their potential use as highly sensitive sensor materials.

Experimental Section

Materials and General Methods. *n*-BuLi, Me_3SiCl, and pyridine (anhydrous grade) were purchased from Acros; BBr_3 was purchased from Aldrich; and C_6F_5Br was purchased from Fluorochem. BBr_3 and C_6F_5Br were distilled under a vacuum prior to use. Pentafluorophenylcopper,[28] trimethylstannylferrocene,[29] *p*-^{t}Bu$C_6H_4SnMe_3$,[30] *p*-^{t}BuC_6H_4-BBr_2,[31] 2,2′-bis(trimethylsilyl)-5,5′-bithiophene (**1a**),[32] and 2,2′-bis-(trimethylstannyl)-5,5′-bithiophene (**1b**)[33] were prepared according to literature procedures for the same or closely related compounds. All reactions and manipulations were carried out under an atmosphere of prepurified nitrogen using either Schlenk techniques or an inert-atmosphere glove box (Innovative Technologies). Ether solvents were distilled from Na/benzophenone prior to use. Hydrocarbon and chlorinated solvents were purified using a solvent purification system (Innovative Technologies; alumina/copper columns for hydrocarbon solvents); the chlorinated solvents were subsequently distilled from CaH_2 and degassed via several freeze−pump−thaw cycles.

All 499.893 MHz ^{1}H, 125.7 MHz ^{13}C, 160.3 MHz ^{11}B, and 470.2 MHz ^{19}F NMR spectra were recorded on a Varian INOVA NMR spectrometer operating at 499.91 MHz. The Varian INOVA 500 spectrometer was equipped with a boron-free probe, and boron-free quartz NMR tubes were used. The 400 MHz ^{1}H, 100.5 MHz ^{13}C, and 79.45 MHz ^{29}Si (DEPT mode) NMR spectra were recorded on a Varian VXR-S spectrometer. All ^{1}H and ^{13}C NMR spectra were referenced internally to solvent signals. ^{11}B NMR spectra were referenced externally to $BF_3{\cdot}Et_2O$ in C_6D_6 ($\delta = 0$), ^{29}Si NMR spectra, to Me_4Si in C_6D_6 ($\delta = 0$), and ^{19}F NMR spectra, to α,α′,α″-trifluorotoluene (0.05% in C_6D_6; $\delta = -63.73$). All NMR spectra were recorded at ambient temperature unless noted otherwise.

UV−visible absorption data were acquired on a Varian Cary 500 UV−vis/NIR spectrophotometer. Solutions were prepared using a microbalance (±0.1 mg) and volumetric glassware and then charged into quartz cuvettes with sealing screw caps (Starna) inside the glove box. The fluorescence data were measured on a Varian Cary Eclipse Fluorescence spectrophotometer with the same solutions as those used in the UV−visible measurements. Anthracene was used as the standard for determination of the quantum yields (Φ). The quantum yield of anthracene was adopted from the *Handbook of Photochemistry*,[34] and the concentration of anthracene in THF was 6.86×10^{-6} M. Titration experiments were performed by successive addition of predetermined amounts of a pyridine solution into the sample quartz cuvette with a sealing screw cap (Starna) using a microliter syringe inside the glove box. After each measurement, the quartz cuvette was returned to the glove box followed by addition of another predetermined amount of the pyridine solution. Binding constants were determined with the program Hyperquad.[35]

Cyclic voltammetry was carried out on a CV-50W analyzer from BAS. The three-electrode system consisted of an Au disk as the working electrode, a Pt wire as the secondary electrode, and a Ag wire as the reference electrode. The voltammograms were recorded with ca. 1.8×10^{-3} M solution in dichloromethane containing $Bu_4N[B(C_6F_5)_4]$ (0.1 M) as the supporting electrolyte. The scans were referenced after the addition of a small amount of decamethylferrocene as the internal standard. The potentials are reported relative to the ferrocene/ferrocenium couple ($E_{1/2} = -610$ mV for decamethylferrocene with respect to ferrocene in dichloromethane).

GC−MS spectra were acquired on a Hewlett-Packard HP 6890 Series GC system equipped with a series 5973 mass selective detector and a series 7683 injector. A temperature profile with a heating rate of 20 °C/min from 50 °C to 280 °C was used. Mass spectral data in FAB positive ion mode with NPOE (2-nitrophenyl octyl ether) or NBA (4-nitrobenzylalcohol) as matrix were obtained at the Michigan State University Mass Spectrometry Facility, which is supported, in part, by a grant (DRR-00480) from the Biotechnology Research Technology Program, National Center for Research Resources, National Institutes of Health. MALDI-TOF−TOF measurements were performed on an Applied Biosystems 4700 Proteomics Analyzer in reflectron mode with

(27) Brown, H. C.; Barbaras, G. K. *J. Am. Chem. Soc.* **1947**, *69*, 1137−1144.
(28) (a) Cairncross, A.; Sheppard, W. A.; Wonchoba, E. *Org. Synth.* **1980**, *59*, 122−131. (b) Sundararaman, A.; Lalancette, R. A.; Zakharov, L. N.; Rheingold, A. L.; Jäkle, F. *Organometallics* **2003**, *22*, 3526−3532.
(29) Guillaneux, D.; Kagan, H. B. *J. Org. Chem.* **1995**, *60*, 2502−2505.
(30) Qin, Y.; Shah, S.; Kiburu, I.; Jäkle, F. *Polym. Prepr.* **2005**, *46* (2), 1026−1027.
(31) Qin, Y.; Cheng, G.; Achara, O.; Parab, K.; Jäkle, F. *Macromolecules* **2004**, *37*, 7123−7131.
(32) Herrema, J. K.; Wildeman, J.; Gill, R. E.; Wieringa, R. H.; van Hutten, P. F.; Hadziioannou, G. *Macromolecules* **1995**, *28*, 8102−8116.
(33) Kamal, M. R.; Al-Taweel, S. A.; El-Abadelah, M. M.; Ajaj, K. M. A. *Phosphorus, Sulfur Silicon Relat. Elem.* **1997**, *126*, 65−74.
(34) Murov, S. L., Carmichael, I., Hug, G. L., Eds. *Handbook of Photochemistry*, 2nd ed.; Marcel Dekker Inc.: New York, 1993.
(35) Gans, P.; Sabatini, A.; Vacca, A. *Talanta* **1996**, *43*, 1739−1753.

Table 5. Experimental Data for the X-ray Diffraction Studies of **4** and **4Py$_2$**

compound	**4**	**4Py$_2$**
empirical formula	$C_{32}H_4B_2F_{20}S_2 \cdot 3\ C_7H_8$	$C_{42}H_{14}B_2F_{20}N_2S_2 \cdot 2\ C_9H_{12}$
M	1130.49	1252.66
T, K	218(2)	100(2)
wavelength, Å	0.71073	1.54178
crystal system	triclinic	triclinic
space group	$P\bar{1}$	$P\bar{1}$
a, Å	7.6711(8)	9.07220(10)
b, Å	11.9741(12)	12.84770(10)
c, Å	13.8819(13)	13.12490(10)
α, deg	93.157(2)	105.5110(10)
β, deg	105.488(2)	100.7860(10)
γ, deg	93.159(2)	105.9210(10)
V, Å^3	1223.7(2)	1360.37(2)
Z	1	1
ρ_{calc}, g cm^{-3}	1.534	1.529
μ, mm^{-1}	0.223	1.893
F(000)	568	634
crystal size, mm^3	0.25 × 0.12 × 0.10	0.17 × 0.14 × 0.09
limiting indices	$-9 \le h \le 9$	$-9 \le h \le 10$
	$-13 \le k \le 14$	$-14 \le k \le 14$
	$-16 \le l \le 16$	$-14 \le l \le 14$
θ range, deg	1.53 to 25.00	3.64 to 59.99
reflns collected	7447	9585
independent reflns	4294 [*R*(int) = 0.0226]	3865 [*R*(int) = 0.0176]
absorption correction	semiempirical from equivalents	semiempirical from equivalents
refinement method	full-matrix least-squares on F^2	full-matrix least-squares on F^2
data/restraints/parameters	4294/18/389	3865/0/392
goodness-of-fit on F^2	1.059	1.029
final *R* indices [$I > 2\sigma(I)$][a]	$R1 = 0.0459$	$R1 = 0.0314$
	$wR2 = 0.1352$	$wR2 = 0.0825$
R indices (all data)[a]	$R1 = 0.0575$	$R1 = 0.0352$
	$wR2 = 0.1427$	$wR2 = 0.0854$
peak/hole (eÅ^{-3})	0.337 and −0.196	0.236 and −0.207

[a] $R1 = \Sigma||F_o| - |F_c||/\Sigma|F_o|$; $wR2 = \{\Sigma[w(F_o^2 - F_c^2)^2]/\Sigma[w(F_o^2)^2]\}^{1/2}$.

delayed extraction. Benzo[*a*]pyrene was used as the matrix (10 mg/mL toluene). Samples were prepared in toluene (10 mg/mL), mixed with the matrix in a 1:10 ratio, and then spotted on the wells of a sample plate inside a glove box. The samples were observed in either positive or negative ion mode as specified. Peptides were used for external calibration **(**Des-Arg-Bradykinin (904.4681), Angiotensin I (1296.6853), Glu-Fibrinopeptide B (1570.6774), ACTH (clip 1−17) (2093.0867), ACTH (clip 18−39) (2465.1989), ACTH (clip 7−38) (3657.9294) with α-hydroxy-4-cyanocinnamic acid as the matrix). Elemental analyses were performed by Quantitative Technologies Inc., Whitehouse, NJ.

X-ray diffraction intensities were collected on a Bruker SMART APEX CCD diffractometer at $T = 218(2)$ (**4**) and 100(2) K (**4Py$_2$**) using MoK$_\alpha$ ($\lambda = 0.71073$ Å) (**4**) and CuK$_\alpha$ (1.54178 Å) (**4Py$_2$**) radiations. Crystallographic data for **4** and **4Py$_2$** and details of X-ray diffraction experiments and crystal structure refinements are given in Table 5. SADABS[36] absorption corrections were applied in both cases. Structures were solved using direct methods and completed by subsequent difference Fourier syntheses and refined by full matrix least-squares procedures on reflection intensities (F^2). In the crystal of **4** there are two solvent toluene molecules, which are disordered over two positions around an inversion center (in ratio 1:1) and in a general position (in ratio 4:1). All non-hydrogen atoms were refined with anisotropic displacement coefficients. The H atoms were placed at calculated positions and were refined as riding atoms. The H atoms of the disordered solvent molecules in **4** were not taken into consideration. The disordered solvent toluene molecules in **4** were refined with restrictions; the typical average values of C−C bond lengths were used in the refinement as targets for corresponding C−C bonds. All software and source scattering factors are contained in the SHELXTL (5.10) program package.[37] Crystallographic data for the structures of **4** and **4Py$_2$** have been deposited with the Cambridge Crystallographic Data Center as supplementary publication no. CCDC-622334 and CCDC-622335, respectively. Copies of the data can be obtained free of charge on application to CCDC, 12 Union Road, Cambridge CB2 1EZ, UK (fax: (+44) 1223-336-033; email: deposit@ccdc.cam.ac.uk).

DFT calculations were performed with the Gaussian03 program as described in ref 22. Excitation data were determined using TD-DFT (B3LYP) calculations.

Caution! BBr_3 is toxic and highly corrosive and should be handled appropriately with great care. Fluorinated grease was used for ground glass joints in reactions involving BBr_3.

Synthesis of (*p*-^{t}BuC$_6$H$_4$)$_2$BBr: A solution of *p*-^{t}BuC$_6$H$_4$SnMe$_3$ (0.97 g, 3.29 mmol) in CH_2Cl_2 (5 mL) was added slowly under stirring to a solution of *p*-^{t}BuC$_6$H$_4$BBr$_2$ (1.00 g, 3.29 mmol) in CH_2Cl_2 (5 mL) at −78 °C. The reaction mixture was allowed to warm up to room temperature in 1 h. All volatile components were removed under a high vacuum. ^{1}H NMR indicated that the product was more than 95% pure. Isolated yield: 0.96 g (81%). ^{1}H NMR ($CDCl_3$, 499.893 MHz): $\delta = 7.99$ (d, $^3J = 8.0$ Hz, 4H, Ph−H$_o$), 7.53 (d, $^3J = 8.0$ Hz, 4H, Ph−H$_m$), 1.39 (s, 18H, Me). ^{13}C NMR ($CDCl_3$, 125.7 MHz): $\delta = 156.9$ (Ph−C$_p$), 137.9 (Ph−C$_o$), 125.1 (Ph−C$_m$), 35.4 (*C*Me$_3$), 31.3 (Me), not observed Ph−C$_i$. ^{11}B NMR ($CDCl_3$, 160.3 MHz): $\delta = 64.8$ ($w_{1/2} = 3000$ Hz).

Reaction of 1b with (*p*-^{t}BuC$_6$H$_4$)$_2$BBr: Synthesis of 3. A solution of (^{t}BuC$_6$H$_4$)$_2$BBr (0.508 g, 1.42 mmol) in CH_2Cl_2 (10 mL) was added slowly under stirring to a solution of **1b** (0.35 g, 0.71 mmol) in CH_2Cl_2 (10 mL). The reaction mixture was left stirring overnight at room temperature. All volatile components were removed under a high

(36) Sheldrick, G.M. *SADABS* (2.01), Bruker/Siemens Area Detector Absorption Correction Program; Bruker AXS: Madison, WI, 1998.

(37) Sheldrick, G. *SHELXTL* (5.10); Bruker XRD: Madison, WI.

vacuum. The crude product was redissolved in hot CH_2Cl_2, and the product was precipitated at −35 °C. Isolated yield: 0.38 g (74%). ^{1}H NMR ($CDCl_3$, 499.893 MHz): δ = 7.72 (d, ^3J = 8.0 Hz, 8H, Ph−H_o), 7.61 (d, ^3J = 4.0 Hz, 2H, Th−H4, 4′), 7.48 (d, ^3J = 4.0 Hz, 2H, Th−H3,3′), 7.45 (d, ^3J = 8.0 Hz, 8H, Ph−H_m), 1.35 (s, 36H, Me). ^{13}C NMR ($CDCl_3$, 125.7 MHz): δ = 154.8 (Ph−C_p), 149.2 (Th−C2,2′), 146.6 (Th−C5,5′), 144.2 (Th−C4,4′), 140.8 (Ph−C_i), 138.5 (Ph−C_o), 127.2 (Th−C3,3′), 125.0 (Ph−C_m), 35.4 (CMe_3), 31.7 (Me). ^{11}B NMR ($CDCl_3$, 160.3 MHz): δ = 59.3 ($w_{1/2}$ = 1500 Hz). UV−vis (CH_2Cl_2, 5.57 × 10^{-7} M): λ_{max} = 411 nm (ϵ = 42 740), 396 nm (ϵ = 48 290). Fluorescence (CH_2Cl_2, 5.19 × 10^{-7} M): $\lambda_{em,max}$ = 436, 461 nm (λ_{exc} = 394 nm), Φ = 0.79. Solid-state fluorescence: $\lambda_{em,max}$ = 472 nm (λ_{exc} = 400 nm), excitation edge λ = 454 nm (λ_{em} = 470 nm). MALDI-TOF−TOF MS (benzo[*a*]pyrene): calcd 718.96, observed (negative mode) 718.54. Elemental analysis for $C_{48}H_{56}B_2S_2$ (718.71) calcd: C, 80.22; H, 7.85. Found: C, 80.52; H, 8.10.

Reaction of 3 with 2 equiv of Pyridine: A solution of pyridine (2.9 mg, 0.037 mmol) in toluene (5 mL) was added dropwise to a solution of **3** (13.4 mg, 0.0186 mmol) in toluene (5 mL). The reaction mixture was kept stirring overnight, which led to formation of a white precipitate. The solid was redissolved in hot toluene, and the product was obtained as a white powdery material at −35 °C. Isolated yield: 13.9 mg (85%). ^{1}H NMR ($CDCl_3$, 499.893 MHz): δ = 8.59 (d, ^3J = 7.0 Hz, 4H, Py−H_o), 8.01 (t, ^3J = 7.0 Hz, 2H, Py−H_p), 7.52 (pst, ^3J = 6.5 Hz, 4H, Py−H_m), 7.26 (d, ^3J = 8.0 Hz, 8H, *t*Bu−Ph), 7.15 (d, ^3J = 8.0 Hz, 8H, *t*Bu−Ph), 7.06, 6.80 (d, ^3J = 3.5 Hz, 2H, Th−H3,3′ and d, ^3J = 3.5 Hz, 2H, Th−H4,4′), 1.31 (s, 36H, Me). ^{11}B NMR ($CDCl_3$, 160.3 MHz): δ = 2.7 ($w_{1/2}$ = 960 Hz). UV−vis (CH_2Cl_2, 5.19 × 10^{-5} M): λ_{max} = 336 nm (ϵ = 23 570). FAB-MS (low-res) with NPOE as matrix: *m*/*z* (%) = 718.4 [M^+ − 2Py] (100).

Reaction of 1a with BBr_3: Synthesis of 2. BBr_3 (4.3 mL, 0.045 mol) was added neat to a solution of **1a** (5.60 g, 0.018 mol) in toluene (200 mL) at −78 °C. The reaction mixture was slowly warmed up to room temperature and heated to 80 °C for 12 h. All volatile components were removed under a high vacuum, and the crude product was recrystallized from toluene to give pale brown crystals. Isolated yield: 5.29 g (57%). ^{1}H NMR ($CDCl_3$, 400 MHz): δ = 7.99 (d, ^3J = 4.0 Hz, 2H, Th−H4,4′), 7.59 (d, ^3J = 4.0 Hz, 2H, Th−H3,3′). ^{13}C NMR ($CDCl_3$, 125.7 MHz): δ = 151.2 (Th−C2,2′), 145.0 (broad, Th−C5,5′), 144.7 (Th−C4,4′), 128.6 (Th−C3,3′). ^{11}B NMR ($CDCl_3$, 160.37 MHz): δ = 47.1 ($w_{1/2}$ = 480 Hz).

Reaction of 2 with 4 equiv of [C_6F_5Cu]: Synthesis of 4. A solution of compound **2** (2.19 g, 4.36 mmol) in toluene (40 mL) was cooled to −78 °C. A solution of [C_6F_5Cu] (3.92 g, 17.0 mmol) in toluene (40 mL) was cooled to −78 °C and then added dropwise over a period of 15 min. The reaction mixture was stirred at −78 °C for 1 h, slowly allowed to warm up to room temperature, and left stirring for 3 h. The reaction mixture was filtered through a fritted glass funnel. All volatile components were removed from the filtrate under a high vacuum, and the remaining yellow solid was recrystallized from a toluene/hexane (9/1) mixture to give the product as bright yellow crystals. Isolated yield: 2.62 g (71%). ^{1}H NMR (CD_2Cl_2, 499.893 MHz): δ = 7.93 (d, ^3J = 4.0 Hz, 2H, Th−H4,4′), 7.73 (d, ^3J = 4.0 Hz, 2H, Th−H3,3′). ^{19}F NMR (470.2 MHz, CD_2Cl_2, 20 °C): δ = −129.1 (m, 8F, Pf−F_o), −149.1 (t, $^3J_{FF}$ = 20 Hz, 4F, Pf−F_p), −160.9 (m, 8F, Pf−F_m). ^{13}C NMR (CD_2Cl_2, 125.7 MHz): δ = 154.2 (Th−C2,2′), 148.4 (Th−C4,4′), 147.2 (dm, $^1J_{CF}$ = 245 Hz, Pf−C_o), 145.5 (Th−C5,5′), 143.7 (dm, $^1J_{CF}$ = 256 Hz, Pf−C_p), 138.3 (dm, $^1J_{CF}$ = 253 Hz, Pf−C_m), 130.2 (Th−C3,3′), 114.4 (t, $^3J_{FF}$ = 30 Hz, Pf−C_i). ^{11}B NMR (CD_2Cl_2, 160.3 MHz): δ = 56.4 ($w_{1/2}$ = 1300 Hz). UV−vis (CH_2Cl_2, 5.85 × 10^{-5} M): λ_{max} = 437 nm (ϵ = 21 850), 413 nm (ϵ = 31 400). Fluorescence (CH_2Cl_2, 5.85 × 10^{-5} M): $\lambda_{em,max}$ = 476 nm, 495 nm (sh) (λ_{exc} = 413 nm), Φ = 0.03. Solid-state fluorescence: $\lambda_{em,max}$ = 525 nm (λ_{exc} = 415 nm), excitation edge 503 nm (λ_{em} = 525 nm).

Reaction of 4 with 2 equiv of Pyridine: Upon addition of pyridine (37.8 μL, 0.47 mmol) to a solution of **4** (200 mg, 0.23 mmol) in CH_2Cl_2 (4 mL) the color changed from dark yellow to colorless. The mixture was layered with hexanes (10 mL) and kept at −35 °C to obtain colorless crystals. Isolated yield: 211 mg (89%). ^{1}H NMR ($CDCl_3$, 499.893 MHz): δ = 8.70 (d, ^3J = 6.0 Hz, 4H, Py−H_o), 8.06 (t, ^3J = 7.5 Hz, 2H, Py−H_p), 7.56 (pst, ^3J = 7.5 Hz, 4H, Py−H_m), 7.02 (d, ^3J = 3.5 Hz, 2H, Th−H4,4′), 6.79 (d, ^3J = 3.5 Hz, 2H, Th−H3,3′). ^{19}F NMR (470.2 MHz, $CDCl_3$, 20 °C): δ = −135.5 (m, 8F, Pf−F_o), −161.7 (t, $^3J_{FF}$ = 20 Hz, 4F, Pf−F_p), −168.1 (m, 8F, Pf−F_m). ^{13}C NMR ($CDCl_3$, 125.7 MHz): δ = 148.2 (dm, $^1J_{CF}$ = 249 Hz, Pf−C_o), 147.2 (Py−C_o), 142.3 (Th−C4,4′), 140.3 (Th−C2,2′), 140.2 (dm, $^1J_{CF}$ = 255 Hz, Pf−C_p), 137.5 (dm, $^1J_{CF}$ = 248 Hz, Pf−C_m), 133.6 (Py−C_p), 125.9 (Py−C_m), 124.1 (Th−C3,3′), 120.3 (b, Py−C_i). ^{11}B NMR (CD_2Cl_2, 160.3 MHz): δ = −2.6 ($w_{1/2}$ = 400 Hz). UV−vis (CH_2Cl_2, 2.55 × 10^{-5} M): λ_{max} = 325 nm (ϵ = 17 400). FAB-MS (low-res) with NPOE as matrix: *m*/*z* (%) = 1012.1 [M^+] (20), 933.1 [M^+ − Py] (25), 854.0 [M^+ − 2Py] (42); also observed: *m*/*z* (%) = 2024.4 [M_2^+] (0.15), 1946.1 [M_2^+ − Py] (0.11).

Reaction of 2 with 2 equiv of $FcSnMe_3$ and then 2 equiv of [C_6F_5Cu]: Synthesis of 5. A solution of **2** (3.62 g, 7.15 mmol) in toluene (150 mL) was added slowly under stirring to a solution of $FcSnMe_3$ (4.90 g, 14.02 mmol) in toluene (100 mL) at −35 °C. The mixture was allowed to warm up slowly and left stirring at room temperature overnight. All volatile components were removed under a high vacuum. The spectroscopic purity of the solid residue was >95% by ^{1}H NMR. The product was used without further purification for the next step. Isolated yield: 4.90 g (96%). ^{1}H NMR ($CDCl_3$, 499.893 MHz): δ = 8.01 (d, ^3J = 4.5 Hz, 2H, Th−H4,4′), 7.53 (d, ^3J = 4.5 Hz, 2H, Th−H3,3′), 4.92, 4.87 (br, 4H, Cp−H2,5 and br, 4H, Cp−H3,4), 4.20 (s, 10H, C_5H_5). ^{13}C NMR ($CDCl_3$, 125.7 MHz): δ = 146.9 (Th−C2,2′), 142.6 (br, Th−C5,5′), 142.0 (Th−C4,4′), 126.7 (Th−C3,3′), 77.6, 77.2 (Cp−C2,5 and Cp−C3,4 overlap with $CDCl_3$ signals), 71.0 (C_5H_5). ^{11}B NMR ($CDCl_3$, 160.3 MHz): δ = 50.5 ($w_{1/2}$ = 1100 Hz). A solution of [C_6F_5Cu] (1.09 g, 4.73 mmol) in toluene (20 mL) was added dropwise at −35 °C to a portion of the bromoborane (1.70 g, 2.38 mmol) in toluene (20 mL) under stirring. The mixture was allowed to warm up, left stirring for 3 h, and then filtered through a fritted glass funnel. All volatile components were removed under a high vacuum. The crude product was purified by recrystallization from a toluene/hexane mixture (2:1) to give a dark red powdery material. Isolated yield: 1.63 g (77%). ^{1}H NMR ($CDCl_3$, 499.893 MHz): δ = 7.48, 7.47 (d, ^3J = 3.5 Hz, 2H, Th−H3,3′ and d, ^3J = 3.5 Hz, 2H, Th−H4,4′), 4.96 (br, 4H, Cp−H3,4), 4.57 (br, 4H, Cp−H2,5), 4.28 (s, 10H, C_5H_5). ^{19}F NMR (470.2 MHz, $CDCl_3$, 20 °C): δ = −130.4 (m, 4F, Pf−F_o), −155.2 (t, $^3J_{FF}$ = 20 Hz, 2F, Pf−F_p), −163.1 (m, 4F, Pf−F_m). ^{13}C NMR ($CDCl_3$, 125.7 MHz): δ = 147.3 (Th−C2,2′), 146.1 (dm, $^1J_{CF}$ = 242 Hz, Pf−C_o), 143.4 (Th−C5,5′), 142.5 (Th−C4,4′), 141.3 (dm, $^1J_{CF}$ = 254 Hz, Pf−C_p), 137.5 (dm, $^1J_{CF}$ = 252 Hz, Pf−C_m), 126.7 (Th−C5,5′), 116.1 (t, $^2J_{CF}$ = 32 Hz, Pf−C_i), 77.4 (Cp−C2,3,4,5), 73.5 (br, Cp−C_i), 70.4 (C_5H_5). ^{11}B NMR ($CDCl_3$, 160.3 MHz): δ = 50.5 ($w_{1/2}$ = 1700 Hz). UV−vis (CH_2Cl_2, 9.44 × 10^{-5} M): λ_{max} = 387 nm (ϵ = 23 890), 524 nm (ϵ = 9350). MALDI-TOF−TOF MS (benzo[*a*]pyrene): calcd 889.99, observed (negative mode) 890.02. CV vs Fc/Fc^+ (CH_2Cl_2, 1.8 × 10^{-3} M): $E_{1/2}$ = −11 mV (ΔE_p = 87 mV); $E_{1/2}$ = 207 mV (ΔE_p = 158 mV).

Reaction of 5 with Pyridine: A solution of pyridine (78 mg, 0.99 mmol) in toluene (10 mL) was added dropwise to a solution of **5** (200 mg, 0.225 mmol). The reaction mixture was kept stirring overnight, which led to formation of an orange precipitate. The solid was redissolved in hot toluene, and the product was obtained as an orange powdery material at −35 °C. Isolated yield: 216 mg (92%). ^{1}H NMR ($CDCl_3$, 499.893 MHz): δ = 8.32 (d, ^3J = 7.5 Hz, 4H, Py−H_o), 7.46, 7.28 (d, ^3J = 3.5 Hz, 2H, Th−H3,3′ and d, ^3J = 3.5 Hz, 2H, Th−H4,4′), 6.59 (t, ^3J = 7.5 Hz, 2H, Py−H_p), 6.20 (pst, ^3J = 7.5 Hz, 4H, Py−H_m), 4.28 (br, 4H, Cp−H3,4), 4.14 (br, 4H, Cp−H2,5), 4.06 (s, 10H, C_5H_5). ^{19}F NMR (470.2 MHz, $CDCl_3$, 20 °C): δ = −129.6 (m, 4F, Pf−F_o), −159.3 (b, 2F, Pf−F_p), −164.8 (m, 4F, Pf−F_m). ^{11}B NMR

($CDCl_3$, 160.3 MHz): $\delta = -3.1$ ($w_{1/2} = 800$ Hz). FAB-MS (low-res) with NBA as matrix: m/z (%) = 890.0 [$M^+ - 2Py$] (100). UV−vis (CH_2Cl_2, 3.70×10^{-5} M): $\lambda_{max} = 329$ nm ($\epsilon = 13\,200$), 393 nm ($\epsilon = 3400$). CV vs Fc/Fc^+ (CH_2Cl_2, 1.8×10^{-3} M): $E_{1/2} = -123$ mV ($\Delta E_p = 135$ mV); $E_{1/2} = -15$ mV ($\Delta E_p = 145$ mV).

Acknowledgment. Acknowledgment is made to the National Science Foundation (NSF CAREER Award CHE-0346828 to F.J. and NSF-CRIF 0443538), to the donors of the Petroleum Research Fund, administered by the American Chemical Society, and to the Rutgers Research Council for support of this research. F.J. is an Alfred P. Sloan research fellow. We thank Dr. Lourderaj and Dr. Balamurugan for helpful discussions.

Supporting Information Available: Crystallographic data for **4** and **4Py$_2$**, a plot of the extended structure of **4**, pyridine titration plots for **3**, and detailed results of the DFT calculations. Complete ref 22. This material is available free of charge via the Internet at http://pubs.acs.org.

JA064396B